Advanced Fiber Materials
https://doi.org/10.1007/s42765-022-00249-1

RESEARCH ARTICLE

Control of Surface Wrinkles on Shape Memory PLA/PPDO Micro-nanofibers and Their Applications in Drug Release and Anti-scarring

Lu Wang[1] · Jingyi Ma[2] · Tao Guo[1] · Fenghua Zhang[1] · Aimeng Dong[2] · Shiqi Zhang[2] · Yanju Liu[3] · Huiping Yuan[2] · Jinsong Leng[1]

Received: 7 October 2022 / Accepted: 18 December 2022

Abstract

Micro- and nano-fibers of shape memory polymers (SMP) offer multiple advantages like high specific surface area, porosity, and intelligence, and are suitable for biomedical applications. In this study, biodegradable poly (p-dioxanone) (PPDO) materials were incorporated to improve the brittleness of shape memory polylactic acid (PLA), and plasticizers were used to reduce the transition temperature of SMP composites such that their transitions could be induced close to body temperature. Furthermore, an electrostatic spinning technology was applied to prepare SMP fibers with wrinkled structures and regulate their microstructures and morphologies such that the intelligent transition of wrinkled and smooth morphologies can be achieved on the fiber surface. The application of this controllable-morphology fiber membrane in intelligent controlled drug release and scar inhibition after Ahmed Glaucoma Valve (AGV) implantation was also studied. The drug release from the stretched and deformed drug-loaded fiber membranes was faster than those from membranes with the original shape. This membrane with micro- and nano-fibers had good anti-scarring effects that improved after drug loading. The achievement of intelligent controlled drug release and the evident anti-scarring effects of the membrane broaden the application of SMP fibers in the biomedical field.

Keywords Shape memory polymers · Micro-nano fibers · Wrinkled structure · Smart controlled release of drugs · Anti-scarring

Introduction

Shape memory polymers (SMPs) are polymeric smart materials, that respond to external stimuli like heat, magnetism, electricity, and light and can revert to their original shape when the stimulus is removed. Compared with shape memory alloys, SMPs offer advantages like lighter weight and higher deformation and are used extensively in aerospace, smart manufacturing, flexible electronics [1, 2], biomedical applications [3], and other fields [4–7]. As the demand for precision manufacturing and small devices grows in various research fields, smart deformable materials like SMPs are also being developed toward micro- and nano-sized materials, including micro- and nano-particles, foams, and fibers [8, 9]. Because of their high specific surface areas and porosity, micro- and nano-fibers have excellent benefits in biomedical applications, such as drug release, tissue engineering, and bioscaffolds[10, 11]. Therefore, the study of

Lu Wang and Jingyi Ma contributed equally to the work.

✉ Fenghua Zhang
fhzhang_hit@163.com

✉ Huiping Yuan
yuanhp2013@126.com

✉ Jinsong Leng
lengjs@hit.edu.cn

[1] Centre for Composite Materials and Structures, Harbin Institute of Technology (HIT), No.2 Yikuang Street, Harbin 150080, People's Republic of China

[2] The Department of Ophthalmology, The Future Medicine Laboratory, The Second Affiliated Hospital of Harbin Medical University, No.246 Xuefu Street, Harbin 150086, People's Republic of China

[3] Department of Astronautic Science and Mechanics, Harbin Institute of Technology (HIT), No. 92 West Dazhi Street, Harbin 150001, People's Republic of China

Published online: 10 January 2023

shape memory micro- and nano-fibers is vital for developing smart micro- and nano-materials.

Electrospinning is a common method for preparing micro-nanofibers, which is simple to operate and control [12]. In 2005, Cha et al. [13] first adopted this technique to fabricate shape memory polyurethane nano-fibers. In 2012, Gong et al. [14] replaced the flat plate receiver normally used in electrostatic spinning with a drum receiver and prepared shape memory polymer fibers (SMPFs) with an oriented structure. Research on multi-functional SMPFs has since progressed significantly. Zhang et al. [15] used electrostatic spinning to prepare Nafion/Fe_3O_4 composite fiber membranes, the shape fixation and recovery ratios of which were both greater than 90%. These membranes also showed multiple shape memory effects (SME). The structure of SMPFs confers on them significant advantages in biomedical applications. Lv et al. [16] used electrostatic spinning technology to fabricate a novel SMPU/ hyaluronic acid bionic composite fiber that could be used for drug release. Moreover, hyaluronic acid doping was beneficial for the biodegradation and drug release of the composite fiber. Chen et al. [17] combined 3D printing, freeze-drying, and cross-linking technologies to successfully fabricate pore-size-controllable gelatin/poly(lactic-co-glycolic acid) electrospun fiber scaffolds, which successfully aided chondrocyte regeneration. Recently, Liverani et al. [18] used the electrostatic spinning technique to produce shape-memory poly (ε-caprolactone) (PCL) fibers loaded with bioactive glass (BG) that possessed excellent shape-memory properties. BG particles allowed the composite nano-fiber to have in vitro bioactivity without inhibiting cell viability. This indicates that SMPFs are of key research value in the biomedical field.

As the technology has developed, research attention has been increasingly focused on the regulation of fiber microstructure and morphology [19, 20]. Since fibers are processed and shaped by a spinning solution, the fiber structure will be affected by the nature of the spinning solution [21]. The types of spinning needles and receiver devices also have an effect on the fibers [20, 22]. Meanwhile, parameters like voltage, propulsion speed, temperature, and humidity should affect the microstructures and morphologies of fibers during the spinning process [19, 23]. The surface of fibers spun with highly volatile solvents is relatively rough and may exhibit porous, wrinkled, or groove structures, among others. Under fixed spinning conditions, the ambient humidity directly affects the nature of the medium around the jet at the needle. When highly volatile solvents and hydrophobic polymers are used, electrostatic spun fibers with rough surfaces and porous structures can be obtained because of the phase separation and curing of the non-solvent-induced polymer solution jet, and the ambient humidity will be changed, which in turn affects the solvent volatilization rate, thereby regulating the fiber surface morphology. In addition, electrostatically spun fibers with rough surfaces are obtained by mixing different types of polymers in the same highly volatile solvent. As different polymer solutions in the jet have different rates of phase separation and curing, the fiber surface morphology can be regulated by varying the spinning solution concentration [24]. Research on the microstructures and surface morphologies of SMPFs should promote the development of smart fiber materials, expand the SMP structures, and promote the development of multi-structural, multi-functional, and intelligent materials.

Based on this research, a biodegradable material poly(p-dioxanone) (PPDO) was introduced herein to improve the brittleness of polylactic acid (PLA), and plasticizers were used to reduce the transition temperature of SMP composites such that their transitions could be induced close to body temperature [25, 26]. Furthermore, electrostatic spinning is adopted to fabricate SMP fibers with wrinkled structures and regulate their microstructures and morphologies to realize the intelligent transformation of wrinkled and smooth fiber surface morphologies. Furthermore, the application of this controllable-morphology fiber membrane was investigated in the intelligent controlled release of mitomycin C (MMC). The drug-loaded fibrous membrane was stretched and deformed above the transition temperature, and then cooled and fixed. Due to the unfolding of the wrinklings, the drug release rate of the stretched fiber membrane was faster than that of the unstretched membrane. When the temperature was raised above the transition temperature, the shape of the fiber recovered to wrinkled, and the drug release rate reduced. And the SMP fiber membrane had the inhibition of scarring of the filtering bleb produced after glaucoma drainage device implantation to broaden the scope of biomedical applications of SMP fibers. (The schematic diagram of the research process is shown in Scheme 1).

Experimental Section

Materials

Polylactic acid (PLA) was acquired from Natureworks LLC (USA) with the product code PLA 4032D. Polydioxanone (PPDO) was provided by BASF AG (Germany). Tributyl citrate (TBC, > 98%) was bought from Aladdin Reagents Ltd. Dichloromethane (DCM) (Analytical Reagent) was obtained from Tianjin Fuyu Fine Chemical Co., Ltd (China). N,N-dimethylformamide (DMF, ≥ 99.9%) (Molecular biology grade) was supplied by Tianjin Fengchuan Chemical Reagent Technology Co., Ltd (China). Phosphate-buffered saline (PBS, without calcium and magnesium) was procured from Shanghai Aladdin Biochemical Technology Co., Ltd (China). MMC was bought from Shanghai Anhui Pharmaceutical Co., Ltd (China).

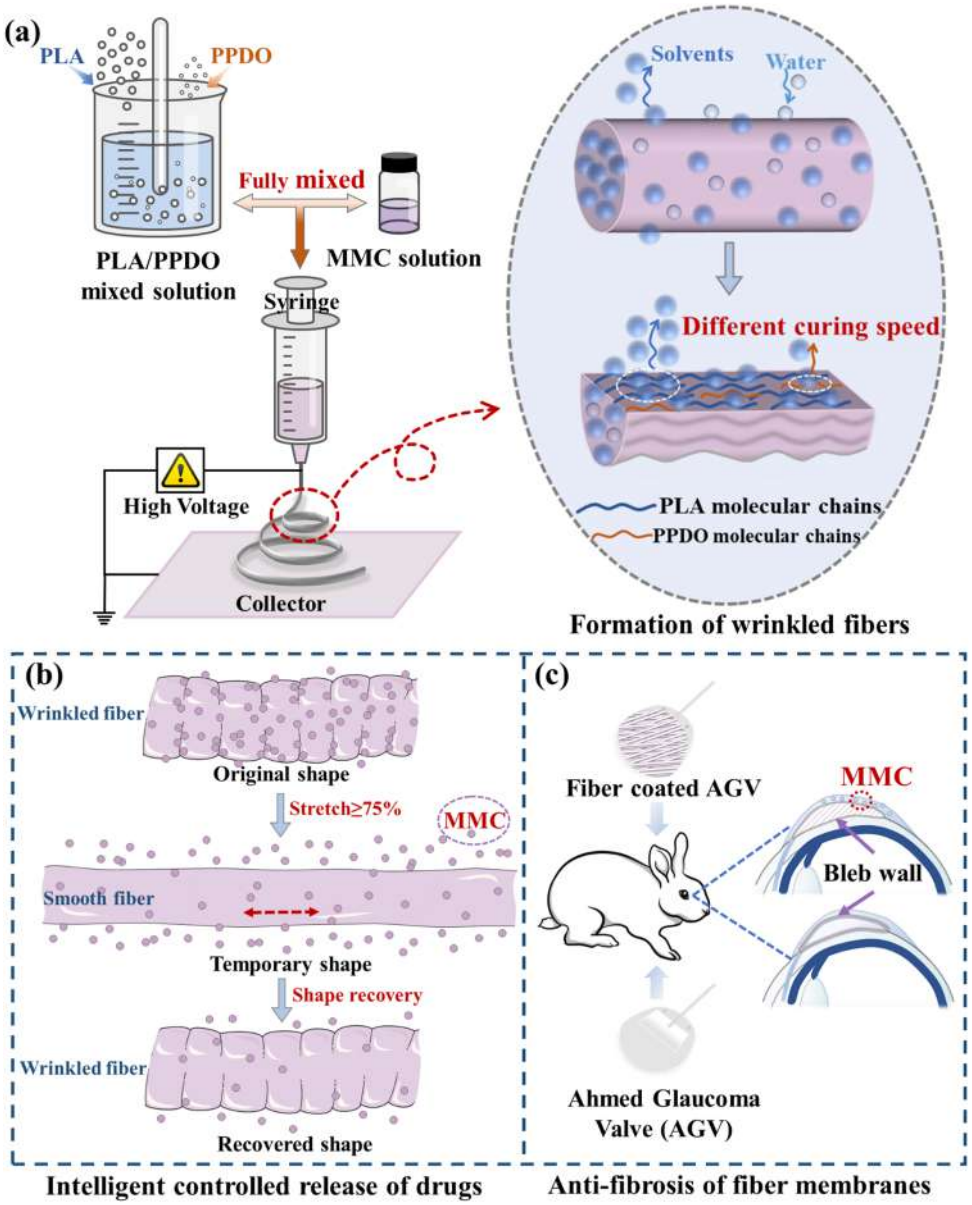

Scheme 1 The schematic diagram of the research process. **a** Electrospinning and formation of PLA/PPDO wrinkled fibers, **b** Intelligent controlled release of drugs, **c** Anti-scarring effect of fiber membranes

Preparation and Characterization of Shape Memory PLA/PPDO Composites

The raw materials, PLA and PPDO, were dissolved in dichloromethane (20 wt%) at a mass ratio of 9:1 and stirred at 100 rpm for 8 h to produce a PLA9/PPDO1 composite solution. The solution was ultrasonically shaken for 1 h to allow evaporation to a constant weight and thereafter demolded and hot-pressed to produce a PLA9/PPDO1 composite sheet. Five samples of equal mass were weighed and added to 10, 20, 30, 40, and 50 wt% of TBC, followed by dissolution in dichloromethane (20 wt%). The solutions were stirred at 100 r/min for 4 h to produce a PLA/PPDO/TBC composite solution. Eventually, the plasticized PLA/PPDO composite sheet ($20 \times 20 \times 2$ mm) was obtained after evaporation (22 °C), demolding, and hot-pressing (60 °C).

Differential scanning calorimetry (DSC, Mettler Toledo, Switzerland), dynamic mechanical analysis (DMA, Waters, USA), and shape memory performance tests were then performed on the samples. The temperature range of DSC was 0–200 °C, and the heating rate was 10 °C/min. The tensile mode was used in the DMA tests. The temperature range of the DMA test was 20–140 °C, the heating rate was 5 °C/

min, and the test frequency was 1 Hz. The shape fixation ratio (R_f), shape recovery ratio (R_r), and recovery rate of the samples were determined during the shape memory performance tests.

An in vitro cytotoxicity assay was performed on the samples. Primary culture and cell passages were performed on rabbit conjunctival Tennon's capsule fibroblasts. Third to fifth-generation cells were selected for the experiments. The samples were sterilized by UV irradiation for 30 min, and the cells were grown in 24-well plates at a density of 10^4 cells/well. Transwells (6.5 mm with 8 μm pore) were added to each well on the second day, and samples and blank controls were added to the upper chamber. On days three and five, the medium was replaced by 100 μl 10% cell counting kit-8 (CCK-8) solution for 30 min, and the absorbance of the medium was measured at 450 nm. On day five, the status of the cells was observed under a light microscope, and live/dead cell staining was performed using a fluorescence microscope (Leica DM2500, Germany).

A test for in vivo toxicity was also performed on the samples. The samples were sterilized and implanted under the skin on the backs of C57 mice. After 3 months, the subcutaneous tissues were taken for hematoxylin and eosin (H&E) staining. The control group was sham-operated.

Preparation and Characterization of Shape Memory PLA/PPDO Micro- and Nano-Fiber Membranes

The PLA9/PPDO1 + 40% TBC composite was dissolved in dichloromethane to produce solutions with concentrations of 5–30 wt%. The solution viscosity was tested using a rheometer (DHR-2, Waters, USA) with shear rates in the 0–120 s^{-1} range. The electrostatic spinning (Beijing Fuma, China) process was conducted at a propulsion rate of 3 mL/h, a voltage of 14 kV, a receiving distance of 20 cm, and room temperature. Eventually, microspheres, beads, or fibers were obtained on the receiving cloth. A scanning electron microscope (SEM, SU5000, Hitachi, Japan) was used to observe the spinning products, and the fiber diameters and distributions were measured using Image J software. The mechanical properties of the fiber membrane were tested using a microcomputer-controlled electronic universal testing machine (CMT2103, Shenzhen Sansi, China) with a tensile rate of 10 mm/min and sample dimensions of $12 \times 5 \times 0.1$ mm. The water contact angle of the fiber membrane was tested using a contact angle measuring instrument (JY-82B, KRUSS, Germany). The specific surface area and pore size distribution of the fiber membranes were measured by using a fully automatic rapid specific surface area analyzer (ASAP 2020, Micromeritics, USA).

Preparation of Shape Memory PLA/PPDO Drug-Loaded Fibrous Membrane and its Application in Drug Release

MMC, which is commonly used in glaucoma surgeries, was selected as the experimental drug to validate the anti-scarring function of the device. The PLA9/PPDO1 + 40% TBC composite was dissolved in dichloromethane (22 wt%) to produce a carrier solution. Different masses of MMC were weighed and dissolved in trace amounts of dimethylformamide to produce a drug solution. The two solutions were mixed and stirred in the dark for 48 h to produce the drug-loaded spinning solution. The shape memory PLA/PPDO micro- and nano-fiber membranes loaded with MMC were obtained by electrostatic spinning, with MMC contents of 0.15, 0.3, and 0.4 wt% (relative to the mass of the polymer). The drug-laden fiber membranes were tested by Fourier-infrared absorption spectroscopy (AVATAR360, Nicolet, USA) to confirm that the MMC was successfully loaded and did not affect the molecular structure of the composites.

To validate the drug release function, a UV spectrophotometer (UV7, Mettler Toledo, Switzerland) was used to determine the absorbance of the MMC solution at 365 nm, and a standard curve was plotted. Samples consisting of 40 mg of drug-loaded fiber membranes containing MMC at 0.15, 0.3, or 0.4 wt% were placed in centrifuge tubes containing 40 mL of PBS buffer. The samples were then placed in a thermostatic water bath shaker (SHA-B, Changzhou Jintanliangyou, China) at 37 °C at an oscillation speed of 90 r/min (simulating the environment of the human body). Thereafter, 2 mL of leachate was removed after 6 and 12 h, and at 1, 2, 3, 4, 5, 6, and 7 days. The absorbance was measured to calculate the drug concentration and cumulative drug release rate according to the standard curve. The drug concentration was corrected according to the following formula:

$$C_n' = C_n + \frac{V}{V_0} \sum_{i=1}^{n-1} C_i, \tag{1}$$

where C_n' corrected concentration, C_n concentration measured at time point n, V_0 total volume of the drug release buffer, V volume of sample.

The microinjection pump method was adopted to simulate the aqueous humor flow rate in the drug release experiment. The two ends of an extension tube were connected to a 20-mL syringe filled with the PBS buffer and the inlet end of a needle-type filter (450 mm^2), respectively. The drug-loaded fiber membrane was placed in the filter. The outlet

end of the filter was connected to a centrifuge tube (for collecting daily filtrate). The infusion pump was pre-started to fill the whole device with the PBS buffer and expel any air. The experiment was conducted at 22 °C and protected from light. The specific parameters were as follows: the area of the fiber membrane was 980 mm^2, and the microinjection pump was pushed at a rate of 0.1 mL/h (2.4 mL/d). The absorbance of MMC in the daily filtrate was measured at 365 nm using an enzyme marker. The concentration of MMC in the filtrate was calculated according to the standard curve to plot the daily drug release curve.

Application of Shape Memory PLA/PPDO Micro- and Nano-Fiber Membrane in Scarring Inhibition of Bleb After Glaucoma Drainage Device (GDD) Implantation

Animal studies were conducted with the approval of the Animal Ethics Committee of the Second Affiliated Hospital of Harbin Medical University (SYDW2020-051). Slit lamp microscopy, fundus examinations, and baseline intraocular pressure (IOP) measurements were performed on all rabbits. Twenty-four healthy white rabbits were divided into six groups ($n = 4$/group): the Ahmed Glaucoma Valve (AGV) control group, fiber-coated AGV groups including PLA, PLA9/PPDO1 + 40% TBC (PPT), stretched and deformed PPT, 0.3% MMC-PPT, and stretched and deformed 0.3% MMC-PPT fiber membranes groups. All fibers were UV disinfected for 30 min. The AGV was wrapped with the fiber membranes. The rabbits were intravenously anesthetized using 3% pentobarbital sodium (1 mL/kg). A conjunctival flap was constructed over the superior-temporal side of the eyeball, and Tenon's capsule was bluntly detached backward. AGV was first initiated through the drainage tube by normal saline, sutured with a nonabsorbable suture, and then fixed to the sclera 3.5 mm posterior to the corneoscleral limbus. In addition, a 23G needle was punctured through the sclera into the anterior chamber, a drainage tube was inserted, and the bulbar conjunctiva was sutured. Antibiotic drops were applied 3 times a day for 1 month. The maximum and minimum thickness values of the wall of the filtering bleb were measured by anterior segment optical coherence tomography (AS-OCT) 1 week and 1 month postoperatively. The rabbits were euthanized 1 month postoperatively for pathological observation. The statistical analysis was applied as follows: data were reported as mean ± standard deviation (mean ± SD), and a one-way ANOVA was utilized to compare the groups ($P < 0.05$ was considered statistically significant).

Results and Discussion

Shape Memory PLA/PPDO Composites

PLA has excellent shape memory properties; however, its poor toughness and high transformation temperature have limited its applications in the biomedical field [27–29]. PPDO is also a biodegradable material with good flexibility [30, 31]. To produce composites with good shape memory properties, PLA and PPDO were dissolved in dichloromethane at a mass ratio of 9:1, evaporated, and hot-pressed to produce PLA9/PPDO1 composites. Figure 1a indicates that the first absorption peak in the DSC curve of PLA results from the glass transition of the amorphous part, corresponding to a transformation temperature of 66 °C, which is the temperature at which shape memory behaviors are induced [32]. The transformation temperature of the PLA9/PPDO1 composite is approximately 59.9 °C. The addition of PPDO decreases the transformation temperature of PLA; however, its reduction effects are limited. Furthermore, the addition of too much PPDO may affect the shape memory properties of the composite. Therefore, based on the PLA9/PPDO1 composite, the transformation temperature was further reduced by adding the plasticizer TBC. Figure 1a indicates that the higher the TBC content, the lower the transformation temperature of the composites. When the TBC content is 40 wt%, the transformation temperature for the PLA9/PPDO1/TBC composite decreases to 41.3 °C, which meets the requirements of the transformation being induced close to body temperature and thus has good prospects for biomedical applications.

The shape memory properties of PLA, PLA9/PPDO1, and PLA9/PPDO1 + 40% TBC composites were tested by preparing uniformly sized samples, heating them uniformly, and changing them to a U-shape. The samples were then cooled, and the external force was removed to obtain a temporary "U-shaped" sample. The samples were maintained at room temperature for 12 h to fix the shape. Shape recovery occurred after the sample was reheated, as shown in Fig. 1b. Table 1 lists the data related to shape memory. It can be observed that it takes 60 s for the PLA temporary "U-shaped" part to revert to its initial shape with an R_r value of 96%. Under the excitation of the heat source at 42 °C, the "U-shaped" part of the PLA9/PPDO1 + 40% TBC composite fully recovers within 26 s. Therefore, the plasticized PLA/PPDO composites display excellent shape memory properties and meet the requirements of inducing transformation

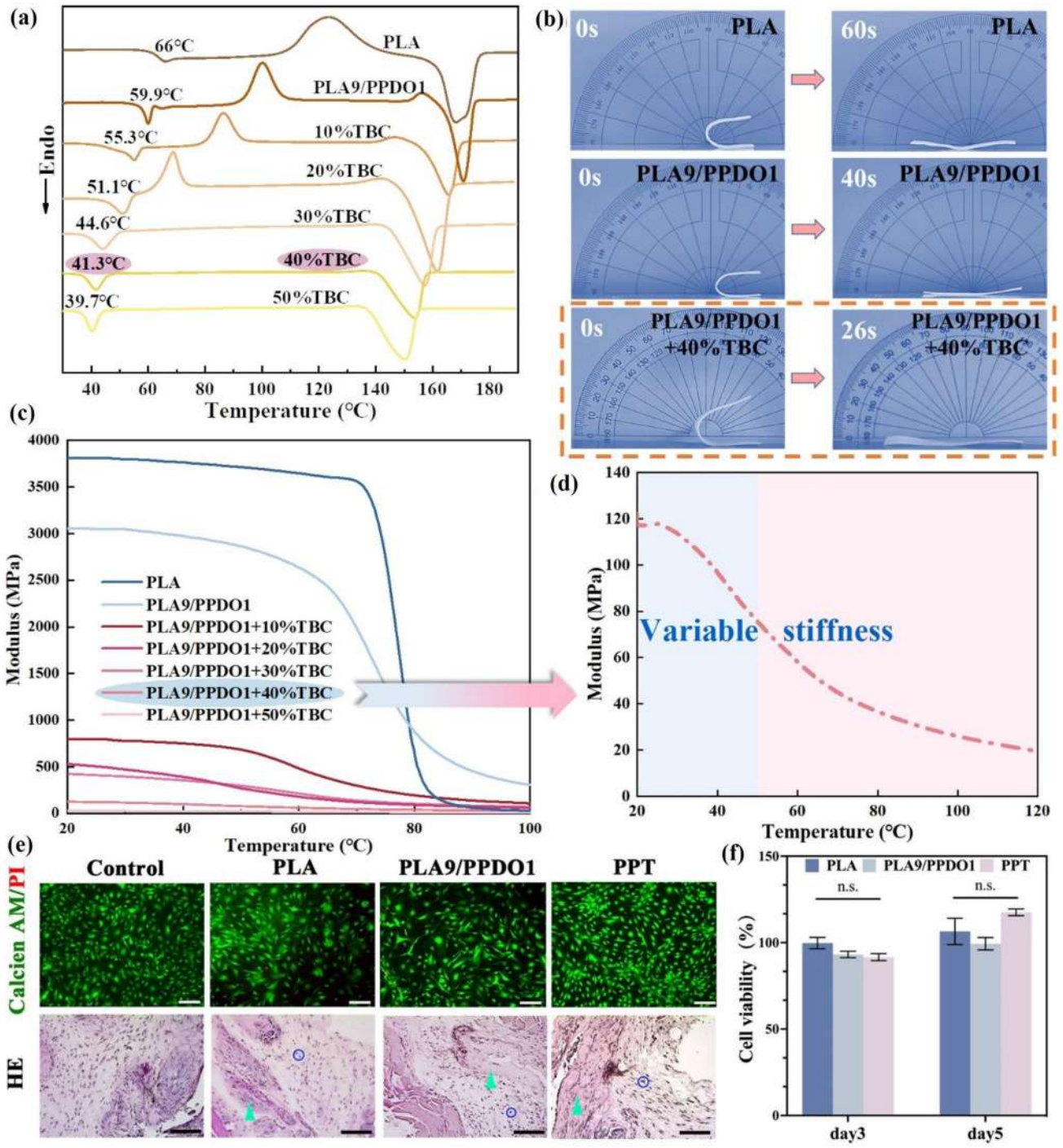

Fig. 1 Characterizations of shape memory materials. **a** DSC test, **b** Shape memory performance test, **c** DMA test (20–140 °C, the heating rate was 5 °C/min), **d** DMA test of PLA9/PPDO1 + 40%TBC composites (20–140 °C, the heating rate was 5 °C/min), **e** Cytocompatibility, histocompatibility of materials: green arrows (fibrous tissue); blue circles (inflammatory cells), **f** Cell viability evaluated by cck-8

close to body temperature. TBC small molecules can promote the crystallization of PLA and increase the proportion of crystalline states in the semi-crystalline polymer PLA. The crystalline state serves as a stationary phase that can thus provide stronger chain segment fixation [18, 33, 34].

Results of the DMA test (Fig. 1c) indicate that the storage modulus of PLA is significant (3800 MPa) at room temperature. Furthermore, the storage modulus of PLA decreases rapidly at 75 °C and is close to zero at 80 °C. This indicates that PLA can maintain significant

Table 1 Shape memory performance data of PLA and PLA/PPDO composites

Material	R_f (%)	R_r (%)	t (s)
PLA	100	96	60
PLA9/PPDO1	100	97.2	40
PLA9/PPDO1 + 40%TBC	97.5	100	26

mechanical strength within a narrow temperature range. PLA is stiffer at low and softer at high temperatures, reflecting the variable stiffness property of shape memory materials [35]. The storage modulus of the composite decreases, and the flexibility increases owing to PPDO. The storage modulus of the PLA9/PPDO1 composite is approximately 3000 MPa at room temperature, indicating the variable stiffness property. Figure 1c indicates that the storage modulus of the composites was greatly reduced by TBC, indicating palpable toughening effects. The TBC small molecules could promote chain segment movement of the polymer, thereby improving the flexibility of the composites [36]. The storage modulus of PLA9/PPDO1 + 40% TBC at room temperature is approximately 120 MPa, which is 1/25 that of PLA9/PPDO1. Moreover, its modulus decreases rapidly at approximately 40 °C (glass transition temperature, T_g), thus exhibiting the variable stiffness property (Fig. 1d). Therefore, by adding the plasticizer, TBC produces a composite system that is more flexible, easier to deform, and more compatible with human tissues.

To validate its biological applicability, the cytotoxicity of the material system was tested, and the results are shown in Fig. 1e. Compared to the blank control group, the in vitro live/dead staining assay showed no significant death of cells within five days, and the growth trends were normal. There was no significant difference in cell viability between the groups (Fig. 1f). In vivo cytotoxicity experiments were performed. The mice all had intact skin on their backs after three months. H&E staining was performed by taking subcutaneous tissues from the wrapped materials. The tissues were dominated by pink stromal tissue, and a small amount of fibrous tissue was observed. Furthermore, no inflammatory cells were evident, and tissue healing was unaffected [37–39]. Thus, the PLA/PPDO/TBC material system is biocompatible.

Shape Memory PLA/PPDO Micro- and Nano-Fiber Membranes

In the electrostatic spinning process, the structure and morphology of fibers are primarily influenced by two parameters: the spinning process and the spinning solution system [16, 40, 41]. The concentration of the spinning solution belongs to the latter category, which affects the structure, morphology, and diameter distribution of the fibers and even directly determines whether the fibers can be formed [42]. For the PLA9/PPDO1 + 40% TBC composite system in this study, when the spinning solution concentration was less than 15 wt%, the spinning products were microspheres or adherent string beads (Fig. 2a). The fibers formed continuously only when the spinning solution concentration was greater than 15 wt%. A three-dimensional network structure formed when the fibers were arranged heterogeneously (Fig. 2b). Meanwhile, the viscosity test indicates that the higher the solution concentration, the higher the viscosity (Fig. S1). When the viscosity is moderate, the droplets are pulled and cleaved into fibers under high pressure. When the viscosity is too high, the electric field force cannot overcome the surface tension and cohesion of the droplets to cleave them into fibers. When the viscosity is too low, the droplets are unstable and cannot create a stable jet to form fibers [43]. The spinning solution concentration also influences the diameter and distribution of the fibers. As demonstrated by measurement statistics of Image J (Fig. 2b), the average diameter of the PLA/PPDO micro- and nano-fibers increased from 3.89 to 8.12 μm as the spinning solution concentration increased from 18 to 30 wt%, and the larger the concentration, the larger the fiber diameter distribution interval. The primary reason for this outcome is that the greater the concentration of the solution, the higher the viscosity of the droplet and the greater its surface tension and cohesion. Under the same electric field, the more viscous the droplet is, the fewer fibers it is cleaved into, and the less stable it is. Hence, the fiber diameters and distribution intervals are larger.

In addition, the effects of the solution concentration on the surface morphology of the fibers were investigated. Figure 2b shows that the wrinkling on the fiber surface first increases as the concentration was increased to 22 wt%s and then decreased as the concentration was increased further. The formation of a surface wrinkling morphology is related to the high-speed motion of the solution in the high-voltage electric field, solvent volatilization, phase separation, and solidification of the solution in the jet. The high-speed motion of the solution jet is subject to electric field traction and repulsion of the surface charge. Meanwhile, surface buckling instability also occurs, which can be affected by the volatilization of the solvent and environmental conditions [44]. The competition between this surface instability and the phase separation and curing rate of the solution in the jet causes the wrinkling of the fiber surface via the mechanism shown in Fig. S2. As the concentration increases, the PLA/PPDO/TBC content in the electrospinning solution increases. Thus, the gap between the different phase separation and curing rates widens, and wrinklings become easy to produce, realizing positive effects. In contrast, with

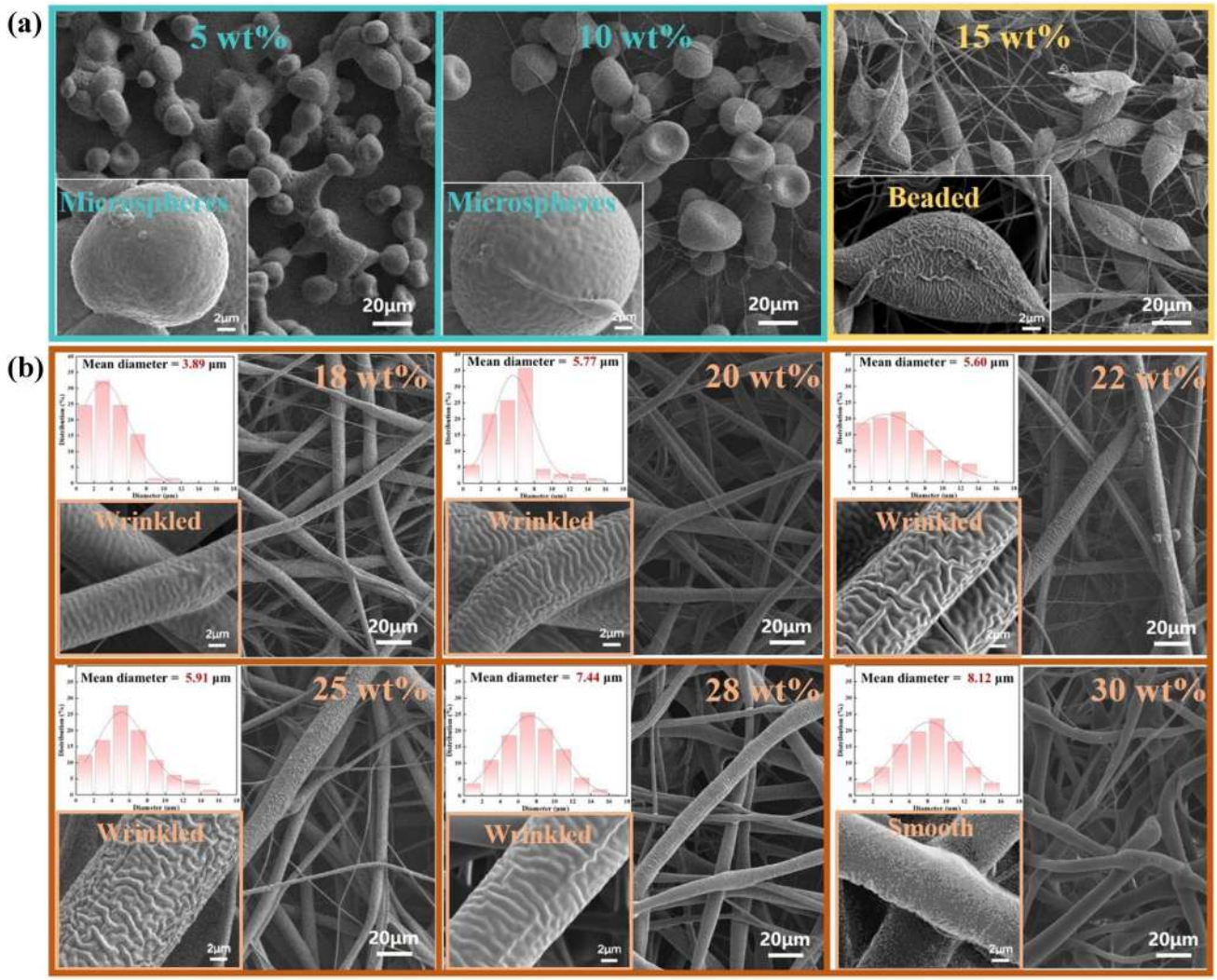

Fig. 2 Effects of PLA9/PPDO1 + 40%TBC solution concentration on fiber structure, diameter, distribution, and surface morphology (The solvent is DCM). **a** SEM images of 5–15 wt% solution spinning products, **b** SEM image and diameter distribution of fibers prepared from 18 to 30 wt% solution

increasing concentration, the solvent content and volatilization decrease, reducing the surface buckling instability and rendering it less likely to produce wrinklings, thereby realizing adverse effects. Therefore, the positive effects of increasing the concentration on deepening wrinkling are greater than the initial negative effects, i.e., the positive effects of further increasing the concentration on this basis are less than the negative effects of increasing the wrinkling. Therefore, with the increase of spinning solution concentration, the wrinkles on the fiber surface first deepened and then decreased.

We selected micro- and nano-fiber membranes with deep surface wrinkles that were prepared by using the PLA9/PPDO1 + 40% TBC spinning solution at a concentration of 22wt% and tested their shape memory, mechanical, water contact angle, specific surface area, and other properties, with a PLA fiber membrane used as the control. First, the macroscopic shape memory performance of the fiber membrane was tested. The transformation temperature of the material system was 41.3 °C, and the long fiber membrane was heated uniformly to 42 °C. Spiral- and U-shapes were made, cooled, and cured. The fiber membranes were then heated to 42 °C and fully reverted within 3 and 5 s, respectively, as shown in Fig. 3a, b. The changes in microstructure and wrinkled surface morphology of the fiber during the shape memory process were further analyzed, and the fiber membrane stretched to assign a shape. Thereafter, SEM was used to observe the fiber membrane before and after stretching and deformation and after reverting to its initial shape. Figure 3c shows the macroscopic shape memory process of the fiber membrane with a heating temperature of 42 °C. The stretched and fixed fiber membrane reverts within 2.6 s

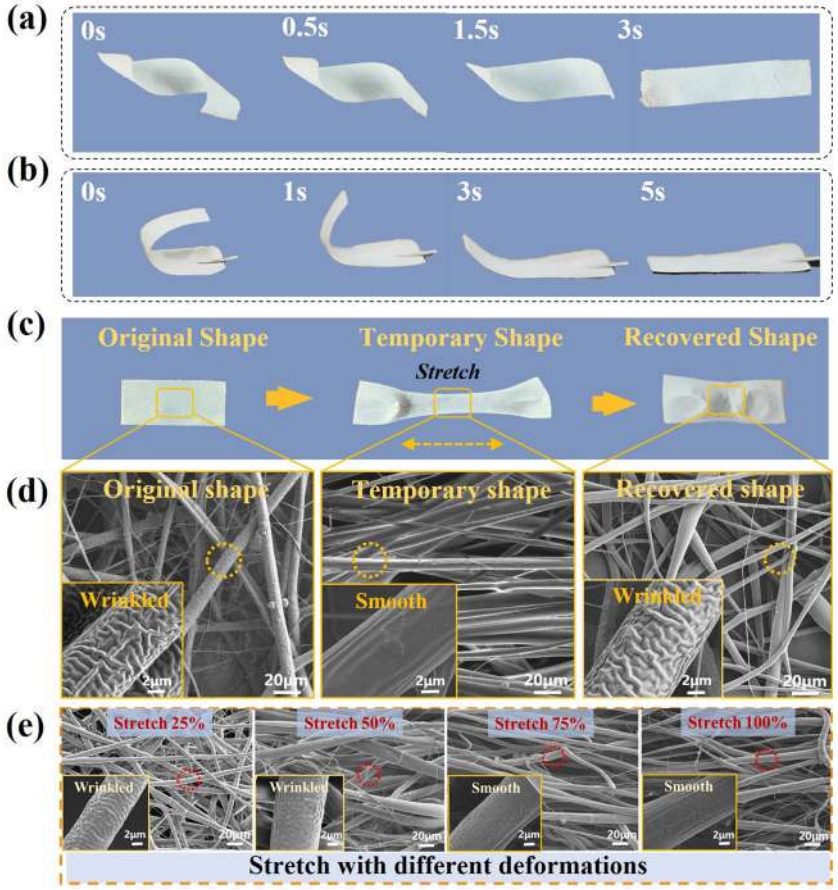

Fig. 3 Shape memory performance test of PLA9/PPDO1 + 40%TBC fiber membranes. Macroscopic shape memory process of **a** Helical, **b** "U"-shaped, and **c** Stretched fiber membranes; **d** Microscopic shape memory process of stretched fiber membrane; e Microstructure of fibers with 25–100% tensile deformation

with $R_r > 90\%$. Figure 3d indicates that the original-shaped fibers were arranged in a disordered manner, with a porous structure between the fibers and a wrinkled structure on the fiber surface. Furthermore, stretching in the horizontal direction can make the fibers oriented and arranged, thus reducing the pores between the fibers. The wrinklings on the fiber surface are pulled apart, thereby exhibiting a relatively smooth shape. After shape recovery, the fibers are no longer oriented, and the porous structure between fibers is recovered, thus returning the fiber surface to a wrinkled shape. We measured the diameter of the fibers before and after stretching and found that the diameter of the fibers became significantly thinner after the tensile deformation(Fig. S3). Figure 3e indicates that the degree of tensile deformation affects the degree of wrinkling on the fiber surface, and the fiber surface is relatively smooth when the deformation exceeds 75%. It can be observed that the macroscopic stretching and shape memory effect can make the surface shape of the fiber switch between wrinkled and smooth; stretching the fiber to different degrees of deformation can regulate the wrinkled morphology of the fiber surface to meet the various application requirements. The wrinkled morphology will increase the specific surface area of the fiber, and its deformation temperature is 41.3 °C, which is close to the body temperature. Hence, this PLA/PPDO micro- and nano-fiber membrane demonstrate a potential for application in intelligent controlled drug release.

Fiber membranes were placed in PBS buffer (37 °C) for 7 days of degradation experiments, and it can be seen from Fig. 4a that they all have good degradability. Among them, PLA9/PPDO1 + 40% TBC fiber membrane has the fastest degradation rate, which is due to the presence of TBC small molecules. Figure 4b shows the stress–strain curves of PLA and PLA9/PPDO1 + 40% TBC fiber membranes with 90 and 89.3% elongation at break point, respectively. The composite fiber membranes exhibited a fracture strength of 1.43 MPa, implying good resilience. Compared with ordinary fibers, micro- and nano-fibers are more suitable for cell growth owing to their large specific surface area and high adsorption capacity [45]. The hydrophobicity of the material itself is

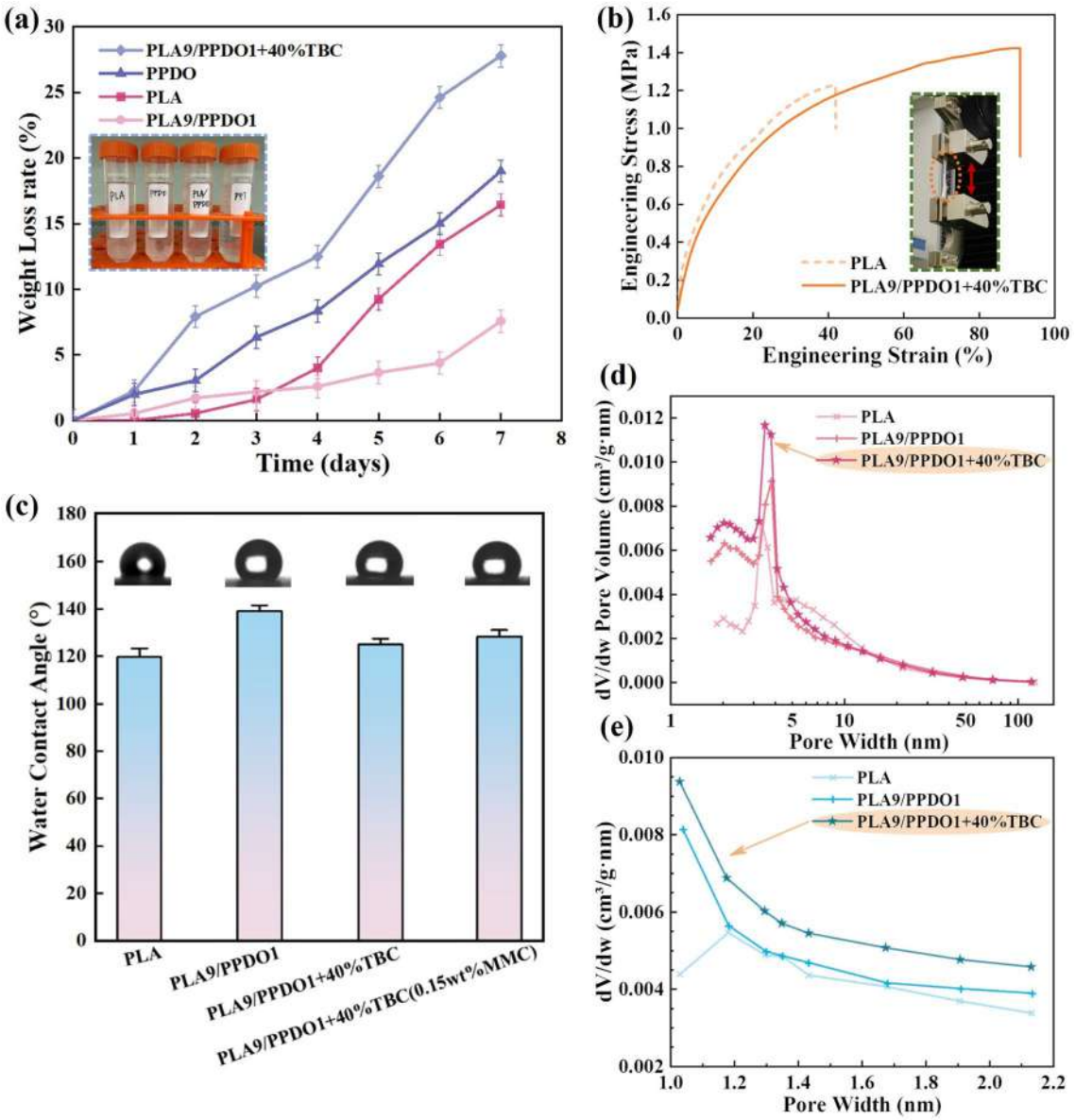

Fig. 4 Characterizations of fiber membranes. **a** Degradation performance test (37 °C), **b** Stress–strain test (the stretch rate was 10 mm/min), **c** Water contact angle test; Pore size distribution curve drawn by **d** BJH and **e** HK method

directly related to cell adhesion. Given the drug release and anti-scarring applications of this fiber membrane, the micro- and nano-fibers are required to be relatively hydrophobic such that they do not exacerbate scar proliferation while releasing the drug. The water contact angle of the fiber membranes was tested (Fig. 4c). Specifically, the water contact angle of the PLA9/PPDO1 fiber membrane was the largest; however, the other membranes were relatively hydrophobic. The water contact angle of the PLA9/PPDO1 + 40% TBC fiber membrane was 125.10 ± 2.37°, which is suitable as a drug-loaded material for inhibiting scarring after glaucoma surgeries.

For drug-loaded fibers, the specific surface area influences drug loading and the drug release rate [46]. Nitrogen adsorption tests were performed on the fibers, and the Barret-Joyner-Halenda (BJH) model was selected to calculate the pore size distribution of the fiber membranes. As shown in Fig. 4d, the PLA9/PPDO1 + 40% TBC fiber membranes have the largest pore volume and number, and a relatively small size, thus creating a peak centered at 4 nm. These pores may result from the unstable volatilization of highly volatile solvents inside the fibers. Furthermore, some fine fibers with nanoscale diameters are staggered, and the voids between them may be filled with nitrogen, thereby equating to a portion of the pores. The Horvath-Kawazoe (HK)

model was used to calculate the microporous pore size distribution of the fiber membranes, as shown in Fig. 4e. There were virtually no micropores in the PLA fiber membranes. In contrast, micropores in the PLA9/PPDO1 + 40% TBC fiber membranes were the most evident, smaller in size, and could effectively increase the specific surface area of the fibers. The specific surface area of each fiber membrane was derived using a BET algorithm. The PLA9/PPDO1 + 40% TBC fiber membrane had the largest specific surface area of 39.3245 m^2/g. The likely reason is that the surface of this fiber is wrinkled, and the average diameter is small (3.6078 μm). The total pore volume and average pore size of the different fiber membranes are listed in Table 2. The PLA9/PPDO1 + 40% TBC fiber membrane with the largest specific surface area has the largest total pore volume and the smallest average pore size, indicating that this fiber membrane has a high specific surface area and porosity.

Shape Memory PLA/PPDO Micro- and Nano-Fiber Membranes for Biomedical Applications

MMC was blended with the PLA9/PPDO1 + 40% TBC solution and electrospun to prepare shape memory micro- and nano-fiber membranes loaded with 0.15, 0.3, and 0.4 wt% MMC. Infrared spectroscopy (Fig. S4) revealed that the addition of MMC did not affect the molecular structure and the chemical stability was sound. Fig. S5 shows the standard concentration curve of MMC, which demonstrates a good linear correlation between its concentration and absorbance within the range of 0–50 μg/mL.

A thermostatic water bath shaker was used to investigate the effects of drug loading on the drug release rate. Figure 5a shows the cumulative drug release curves of shape memory PLA/PPDO micro- and nano-fiber membranes with MMC contents of 0.15, 0.3, and 0.4 wt%. It can be observed from the graphs that the higher the drug loading, the faster the drug release. Furthermore, the cumulative drug release reached equilibrium after approximately 4 days. To further investigate the effects of drug content on the drug release rate, SEM tests were performed on the PLA/PPDO fiber membranes with different MMC contents, and Image J software was used to conduct the quantitative statistical analysis. The results are presented in Fig. 5b. The average diameters of the drug-loaded fiber membranes were smaller than those of the unloaded fiber membranes. In addition, the larger the drug loading, the smaller the fiber diameter and the more uniform the thickness. The likely reason is that, on the one hand, adding the drug solution slightly decreases the concentration of the spinning solution. On the other hand, the drug may make the solution more conductive, and the droplets are more likely to be pulled by high-voltage electricity and cleaved into fibers. Both factors could reduce the diameter of the fiber, increase the specific surface area, and increase the drug release rate.

The experiments demonstrate that the wrinkled surface morphology of this fiber can be changed by macroscopic stretching, which we believe will affect its drug-release behavior. Samples containing 40 mg of MMC-loaded fiber membranes with different MMC contents of 0.15, 0.3, and 0.4 wt% were weighed, heated to 42 °C, and completely stretched and deformed. In this way, the surface wrinklings were completely stretched out. After being cooled and cured, a seven-day drug release experiment was performed (taking the original shape of the fiber membrane with different drug loadings as the control), and the results are shown in Fig. 5c. The drug release rate of the stretched and deformed (smooth surface) membrane was higher than that of the membrane of the original shape (wrinkled surface). The cumulative release reached equilibrium after approximately four days. The higher the drug loading, the smaller the gap in the drug release rate between the two states of the fiber membrane. The possible reason for this result is that stretching changes the surface morphology of the fibers from wrinkled to smooth, thus making for the solvent to infiltrate the fibers, which in turn facilitates the dissolution of the drug molecules hidden in the wrinklings and fibers. Thus, the drug release rate is higher. The stretched and deformed drug-loaded fibers can be placed in the affected area to rapidly release the MMC in a short time and then stimulated by a heat source to recover the shape and achieve a slow release. We used in vitro dynamic drug release to simulate the above process, and found that after excitation of heat source at 42 °C, the drug-loaded fiber membrane slowed down the drug release rate due to shape recovery, and achieved the effect of slow release(Fig. 5d). 0.3 and 0.4 wt% MMC fiber membranes can also achieve controlled drug release, as shown in Fig. S6.

We used the microinjection pump to simulate the flow rate of rabbit ocular aqueous humor in drug release experiments over 16 days. Figure 6a shows the daily drug release curves

Table 2 Comparison of properties of different micro- and nano-fiber membranes

Material	Diameter (μm)	Total pore volume (cm^3/g)	Average pore size (nm)	Specific surface area (m^2/g)
PLA	7.5243	0.064170	8.4611	24.3120
PLA9/PPDO1	6.6179	0.071808	7.4471	33.8243
PLA9/PPDO1 + 40%TBC	3.6078	0.071025	6.3787	39.3245

of the drug-loaded fiber membranes with MMC contents of 0.15, 0.3, and 0.4 wt%. The daily drug release of the fiber membranes gradually decreased. The daily drug release of the 0.4 wt% MMC fiber membrane was basically the same in the first seven days and started to decrease after seven days. The daily release amount decreased from 2.19 to 1.75 μg within 16 days. The higher the drug loading, the faster and more stable the drug release (equal daily release amounts).

The effects of stretching and deformation on the drug-release behaviors of SMPF membranes were also investigated. The drug-loaded fiber membranes were heated and stretched, cooled, and cured. Drug release experiments were performed (taking the original shape of the fiber membranes with different drug loading as the control group), and the results are shown in Fig. 6b–d. The daily drug release of the stretched and deformed (smooth surface) fiber membranes was greater than that of the original shape (wrinkled surface) fiber membranes. The drug release trend was consistent for the fiber membranes in all the groups. The release of the stretched 0.4 wt% MMC fiber membrane was 2.13 μg on day 16, compared with 1.82 μg for the unstretched fiber membranes. Simulation of the ocular environment demonstrates that the drug-loaded

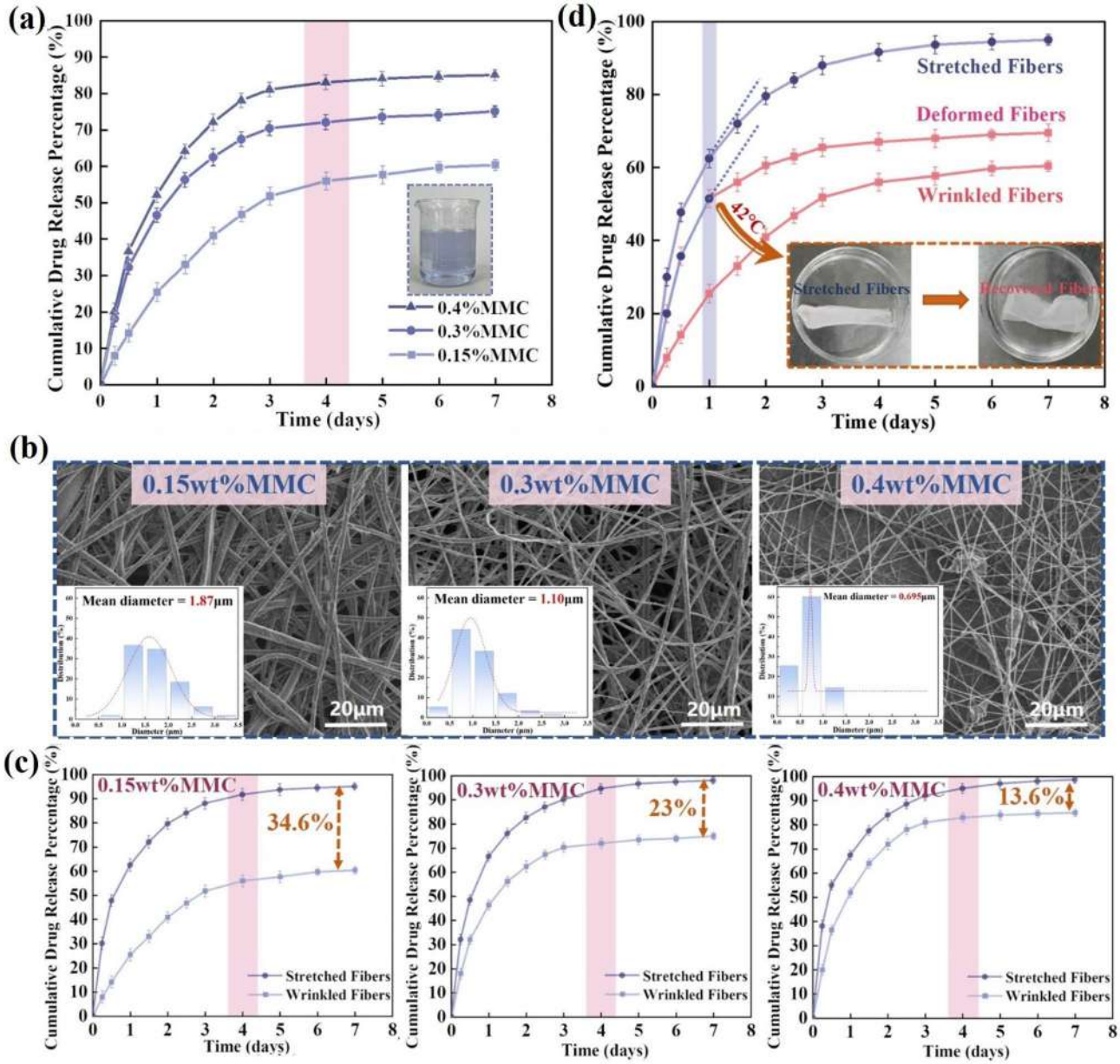

Fig. 5 Application of shape memory PLA/PPDO fiber membranes in drug release (water bath shaker, 37 °C, 90 r/min). **a** Cumulative drug release curves of fiber membranes with different drug loadings, **b** SEM and diameter distribution of drug-loaded fibers, **c** Cumulative drug release curves of unstretched/stretched fiber membranes, **d** Dynamic release process of 0.15 wt% MMC fiber membrane

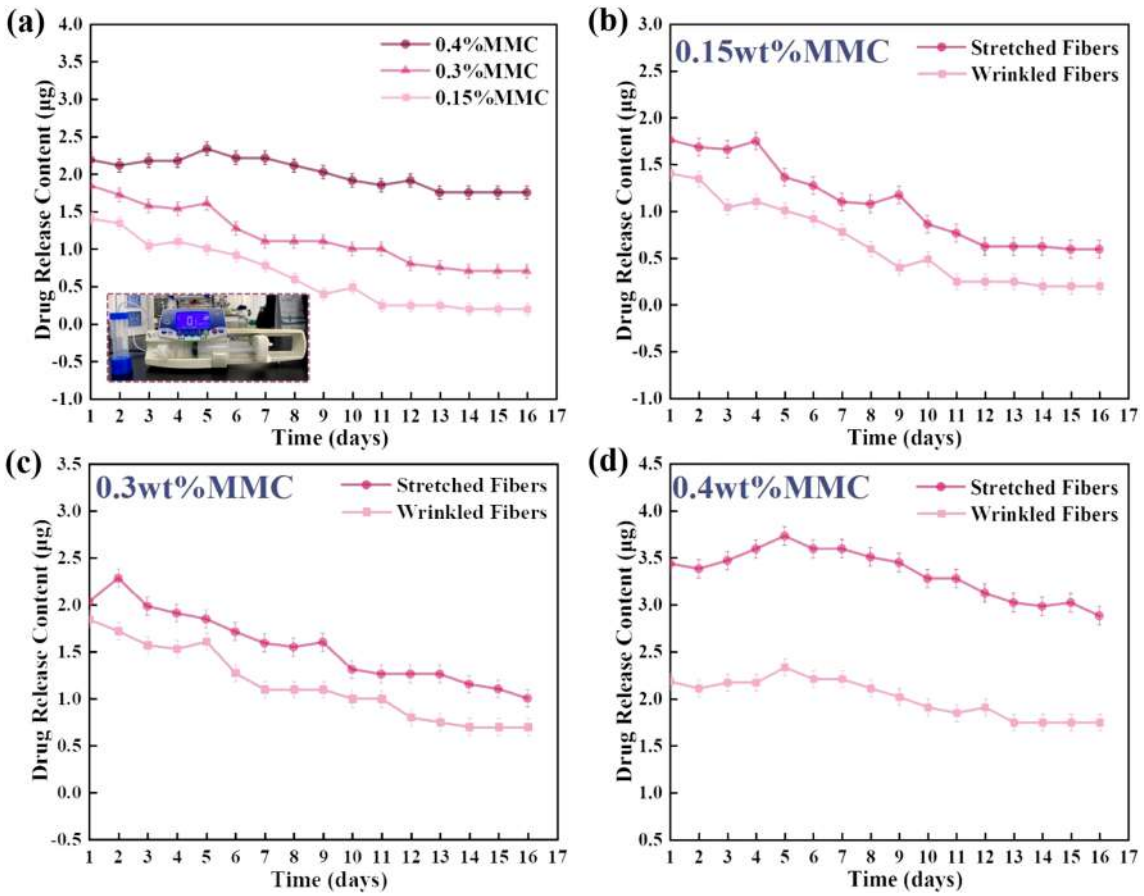

Fig. 6 Daily drug release curves of fiber membranes (microinjection pump method). **a** Different drug loadings, **b–d** Unstretched/stretched fiber membranes

fiber membrane can achieve long-term slow drug release in the eye and exhibit the function of intelligent controlled release.

Anti-glaucoma medication or laser therapy is generally used to treat glaucoma, whereas glaucoma filtration surgery is the preferred procedure in cases where both methods fail to control IOP [47]. GDD implantation is commonly used to treat refractory glaucoma. However, tissue damage repair tends to lead to scarring in the filter channel, preventing aqueous humor outflow and leading to surgery failure. Therefore, scarring inhibition after glaucoma surgeries is crucial to raise the success rate of the surgery [48]. Micro- and nano-fibers can effectively inhibit tissue proliferation owing to their large specific surface area and porosity. MMC is a common therapeutic drug during glaucoma surgeries and has good anti-scarring effects. Thus, unloaded/loaded MMC shape-memory micro- and nano-fiber membranes boast application benefits in scar inhibition in glaucoma surgery [49–51].

AGV control, PLA, PLA9/PPDO1 + 40% TBC (PPT), stretched and deformed PPT, 0.3 wt% MMC-PPT, and stretched and deformed 0.3% MMC-PPT fiber membranes were implanted into rabbit eyes (Fig. 7a). The relevant conditions of the filtering bleb were measured in vivo by AS-OCT. The OCT of the anterior segment allows in vivo observation of the thickness of the filtering bleb wall, patency of the drainage tubes, and whether the cornea and conjunctiva are edematous in rabbit eyes after glaucoma drainage valve implantation. These reflect the biosafety of the implant and specific changes in the thickness of the filtering bleb wall. Figure 7b presents the OCT scans of the filtering bleb wall in rabbits' eyes one week and one month after implantation of the different fiber membranes and indicate that the drains were patent and no significant inflammatory reaction was observed. Compared with the AGV control group, the other groups all exhibited a reduction in the wall thickness of the filtering bleb, with the exception of the PLA group. Moreover, the MMC-PPT group, after stretching and deformation, exhibited the best effects in alleviating scarring. Image J software was used to measure the thickest and thinnest parts of each filtering bleb wall in the OCT scans, and a statistical graph of the maximum and minimum values was obtained, as shown in Fig. 7d and e, respectively. Mild conjunctival edema was observed one week after surgery. The thickness of the drug-loaded group was slightly higher than that of the unloaded group, probably owing

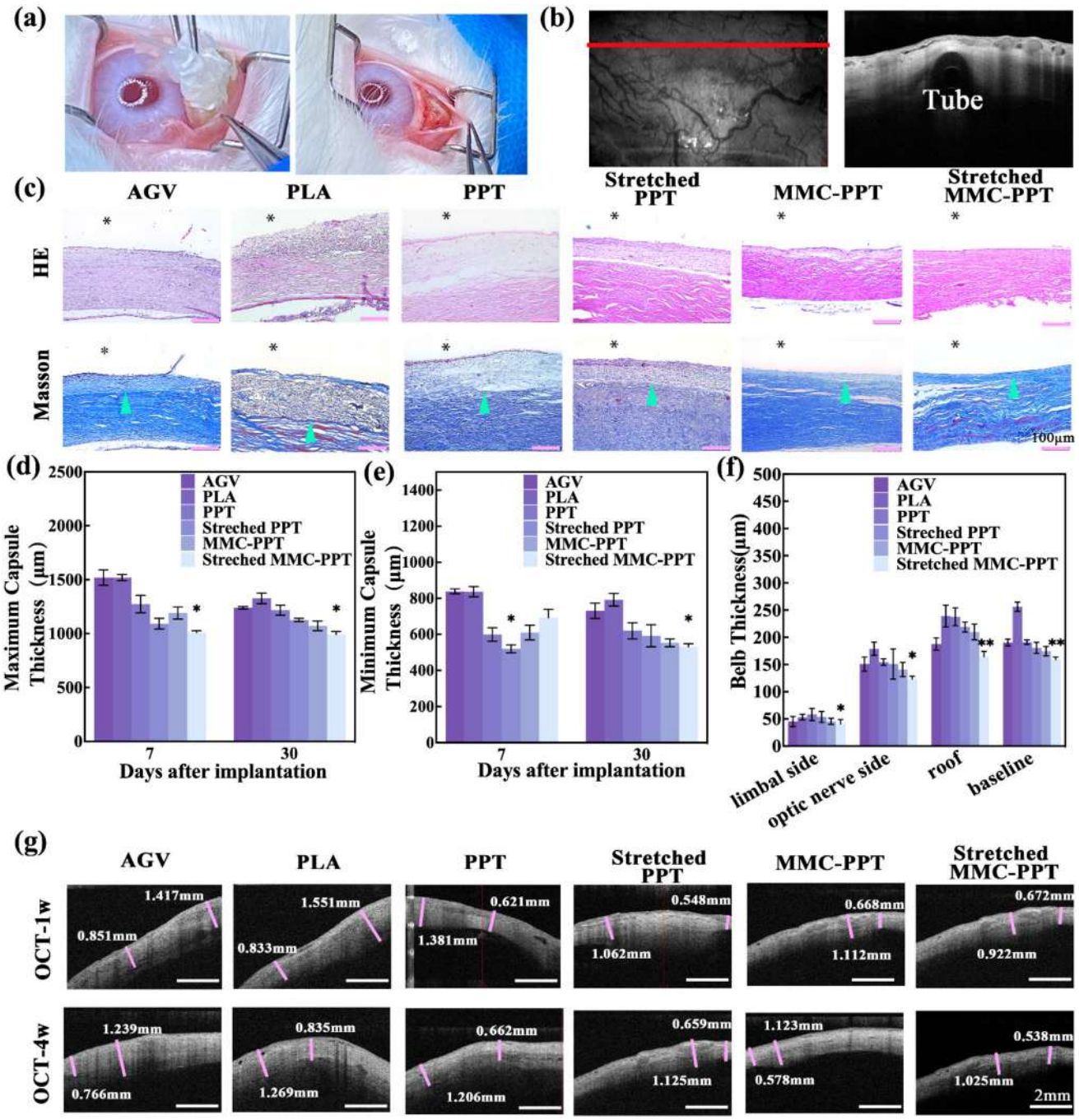

Fig. 7 Shape memory fiber membranes for in vivo anti-fibrosis in AGV implantation. **a** Process of fiber membranes coated AGV implantation, **b** Anterior segment optical coherence tomography (AS-OCT) scan position (red line) and AGV tube condition after operation, **c** H&E and Masson staining of filtering bleb, Scale bar 100 μm; **d**, **e** Maximum and minimum capsule thickness of filter bleb, respectively. $^{*}P<0.05$ as compared to the control ($n=4$), **f** Bleb wall thickness of filtering bleb stained with Masson staining in each group. $^{*}P<0.05$, $^{**}P<0.01$ as compared to the control (n = 4), **g** Representative AS-OCT at postoperative 1 and 4 weeks. Scale bar 2 mm

to the heavier postoperative conjunctival reaction affected by MMC. One month after surgery, the thickness of the filtering bleb wall exhibited varying degrees of decrease in each group, and the conjunctival edema was eliminated; however, the bleb thickness in the PLA group remained higher than that of the control group. The thickness of the filtering bleb in the stretched and deformed MMC-PPT group decreased significantly, and the maximum value was a mere 992.5 ± 26.47 μm.

A pathological observation of the wall of the filtering bleb was also performed. Figure 7c shows a Masson and H&E

stained map of the wall of the filtering bleb at the drainage valve covered with different fiber membranes one month after the implantation. No inflammatory cells were observed in the postoperative pathology, and a denser collagenous fibrous tissue was visible. As demonstrated by Masson's staining, the scar tissue was stained by a more varying degree than the scleral tissue, and the thickness of the filtering bleb was significantly less in the PPT group than in the control group, demonstrating that the fiber could alleviate scarring. Image J software was used to measure the stain map and derived the statistical graph of the filtering bleb wall thickness for each group one month after implantation, as shown in Fig. 7f and g. The scleral surface thicknesses were 190.2 ± 6.319, 256.3 ± 8.310, and 159.0 ± 4.618 μm (mean ± SD) in the AGV control, PLA, and tensile-deformed MMC-PPT groups, respectively. It can be observed that PLA fibers cannot inhibit scar proliferation. In contrast, PPT fibers have sound anti-scarring functions, probably owing to the relative hydrophobicity and wrinkled morphology of the fiber membrane surface. Moreover, stretching and deformation enhance the anti-scarring effects of the fiber membranes. Drug-loaded PPT fiber membranes exhibit better effects in alleviating scarring because of the effects of MMC. Drug-loaded PPT fiber membranes have the best effects in inhibiting scarring because the drug release of the fiber membrane increases after stretching and deformation. The oriented fibers can inhibit tissue growth, thereby reducing the formation of scarring. Therefore, the PLA/PPDO micro- and nano-fiber membrane serve to alleviate the scarring while controlling the drug release intelligently and thus has a good prospect for biomedical applications.

Conclusions

In this study, a shape memory PLA/PPDO composite was designed and fabricated with a transformation temperature of 41.3 °C and meets the requirements of being induced under body temperature. The electrostatic spinning technique prepared shape memory PLA/PPDO micro- and nano-fibers. These fibers have a wrinkled surface morphology, and the SMEs can make the surface morphology of the fibers switch between wrinkled and smooth. Moreover, the fiber membrane has a high specific surface area. The bath oscillation and micro-injection pump methods were used to investigate the function of intelligent controlled drug release of the shape memory micro- and nano-fiber membrane and found that the membrane had good effects on scar inhibition after AGV implantation. In conclusion, this wrinkled-surface shape memory PLA/PPDO micro- and nano-fiber broadens the application scope of SMPFs and has great potential for biomedical intelligence.

Supplementary Information The online version contains supplementary material available at https://doi.org/10.1007/s42765-022-00249-1.

Acknowledgements This work was supported by the National Natural Science Foundation of China (Grant No. 11802075, 12072094, 81870654, and 82070956),the Fundamental Research Funds for the Central Universities (No. IR2021106 and IR2021232), and Applied Technology Research and Development Program of Heilongjiang Provincial Science and Technology Department (GA20C008).

Declarations

Conflict of interest The authors state that there are no conflicts of interest to disclose.

References

1. Wu S, Guo J, Wang Y, Xie H, Zhou S. Cryopolymerized polyampholyte gel with antidehydration, self-healing, and shape-memory properties for sustainable and tunable sensing electronics. *ACS Appl Mater Interfaces* **2022**;*14*:42317–27.
2. Huang J, Wang Y, Guo J, Wu S, Xie H, Zhou S. Anisotropic conductive shape-memory aerogels as adaptive reprogrammable wearable electronics for accurate long-term pressure sensing. *J Mater Chem A* **2022**;*10*:3933–43.
3. Li C, Cui W. 3D Bioprinting of cell-laden constructs for regenerative medicine. *Eng Regen* **2021**;*2*:195–205.
4. Zhang F, Xia Y, Liu Y, Leng J. Nano/microstructures of shape memory polymers: from materials to applications. *Nanoscale Horiz* **2020**;*5*:1155–73.
5. Zhang F, Wang L, Zheng Z, Liu Y, Leng J. Magnetic programming of 4D printed shape memory composite structures. *Compos Part Appl Sci Manuf* **2019**;*125*:105571.
6. Zhang F, Zhao T, Ruiz-Molina D, Liu Y, Roscini C, Leng J, Smoukov SK. Shape memory polyurethane microcapsules with active deformation. *ACS Appl Mater Interfaces* **2020**;*12*:47059–64.
7. Allonas X, Pierrel J, Ibrahim A, Croutxé-Barghorn C. On-demand photopolymerization of fiber-reinforced polymers exhibiting the shape memory effect. *Polymers* **2021**;*13*:4300.
8. Akman R, Ramaraju H, Hollister SJ. Development of photocrosslinked poly(glycerol dodecanedioate)—a biodegradable shape memory polymer for 3D-printed tissue engineering applications. *Adv Eng Mater* **2021**;*23*:2100219.
9. Sarvari R, Keyhanvar P, Agbolaghi S, Gholami Farashah MS, Sadrhaghighi A, Nouri M, Roshangar L. Shape-memory materials and their clinical applications. *Int J Polym Mater Polym Biomater* **2022**;*71*:315–35.
10. Yang X, Wang L, Wang W, Chen H, Yang G, Zhou S. Triple shape memory effect of star-shaped polyurethane. *ACS Appl Mater Interfaces* **2014**;*6*:6545–54.
11. Furtado M, Chen L, Chen Z, Chen A, Cui W. Development of fish collagen in tissue regeneration and drug delivery. *Eng Regen* **2022**;*3*:217–31.
12. Chen H, Zhang F, Sun Y, Sun B, Gu B, Leng J, Zhang W. Electrothermal shape memory behavior and recovery force of four-dimensional printed continuous carbon fiber/polylactic acid composite. *Smart Mater Struct* **2021**;*30*:025040.
13. Cha DI, Kim HY, Lee KH, Jung YC, Cho JW, Chun BC. Electrospun nonwovens of shape-memory polyurethane block copolymers. *J Appl Polym Sci* **2005**;*96*:460–5.
14. Gong T, Li W, Chen H, Wang L, Shao S, Zhou S. Remotely actuated shape memory effect of electrospun composite nanofibers. *Acta Biomater* **2012**;*8*:1248–59.
15. Zhang FH, Zhang ZC, Luo CJ, Lin I-T, Liu Y, Leng J, Smoukov SK. Remote, fast actuation of programmable multiple shape memory composites by magnetic fields. *J Mater Chem C* **2015**;*3*:11290–3.

16. Lv H, Tang D, Sun Z, Gao J, Yang X, Jia S, Peng J. Electrospun PCL-based polyurethane/HA microfibers as drug carrier of dexamethasone with enhanced biodegradability and shape memory performances. *Colloid Polym Sci* **2020**;*298*:103–11.
17. Chen W, Xu Y, Liu Y, Wang Z, Li Y, Jiang G, Mo X, Zhou G. Three-dimensional printed electrospun fiber-based scaffold for cartilage regeneration. *Mater Des* **2019**;*179*:107886.
18. Liverani L, Liguori A, Zezza P, Gualandi C, Toselli M, Boccaccini AR, Focarete ML. Nanocomposite electrospun fibers of poly(ε-caprolactone)/bioactive glass with shape memory properties. *Bioact Mater* **2022**;*11*:230.
19. Yao Y, Xu Y, Wang B, Yin W, Lu H. Recent development in electrospun polymer fiber and their composites with shape memory property: a review. *Pigment Resin Technol* **2018**;*47*:47–54.
20. Shirole A, Sapkota J, Foster EJ, Weder C. Shape memory composites based on electrospun poly(vinyl alcohol) fibers and a thermoplastic polyether block amide elastomer. *ACS Appl Mater Interfaces* **2016**;*8*:6701–8.
21. Zhang F, Zhang Z, Liu Y, Leng J. Shape memory properties of electrospun nafion nanofibers. *Fibers Polym* **2014**;*15*:534–9.
22. Xue J, Wu T, Dai Y, Xia Y. Electrospinning and electrospun nanofibers: methods, materials, and applications. *Chem Rev* **2019**;*119*:5298–415.
23. Qi X, Dong Y, Islam MZ, Zhu Y, Fu Y, Fu S-Y. Excellent triple-shape memory effect and superior recovery stress of ethylene-vinyl acetate copolymer fiber. *Compos Sci Technol* **2021**;*203*:108609.
24. Zhang C, Yuan X, Wu L, Han Y, Sheng J. Study on morphology of electrospun poly(vinyl alcohol) mats. *Eur Polym J* **2005**;*41*:423–32.
25. Gong T, Zhao K, Wang W, Chen H, Wang L, Zhou S. Thermally activated reversible shape switch of polymer particles. *J Mater Chem B* **2014**;*2*:6855–66.
26. Liu C, Xu X, Cui W, Zhang H. Metal-organic framework (mof)-based biomaterials in bone tissue engineering. *Eng Regen* **2021**;*2*:105–8.
27. Wang L, Zhang F, Liu Y, Leng J. Shape memory polymer fibers: materials, structures, and applications. *Adv Fiber Mater* **2022**;*4*:5–23.
28. Guo X, Wei X, Chen Z, Zhang X, Yang G, Zhou S. Multifunctional nanoplatforms for subcellular delivery of drugs in cancer therapy. *Prog Mater Sci* **2020**;*107*:100599.
29. Sun J, Peng B, Lu Y, Zhang X, Wei J, Zhu C, Yu Y. A photoorganizable triple shape memory polymer for deployable devices. *Small* **2022**;*18*:2106443.
30. Lv J, Liu Y, Wei J, Chen E, Qin L, Yu Y. Photocontrol of fluid slugs in liquid crystal polymer microactuators. *Nature* **2016**;*537*:179–84.
31. Chen G, Dong J, Xu X, Zou W, Jin B, Peng W, Zhao Q, Xie T, Zheng N. Converse two-way shape memory effect through a dynamic covalent network design. *J Mater Chem A* **2022**;*10*:10350–4.
32. Zhao Q, Qi HJ, Xie T. Recent progress in shape memory polymer: new behavior, enabling materials, and mechanistic understanding. *Prog Polym Sci* **2015**;*49–50*:79–120.
33. Wei W, Zhang P, Cao F, Liu J, Qian K, Pan D, Yao Y, Li W. Ultrathin Flexible electrospun EVA nanofiber composite with electrothermally-driven shape memory effect for electromagnetic interference shielding. *Chem Eng J* **2022**;*446*:137135.
34. Zhang Q, Rudolph T, Benitez AJ, Gould OEC, Behl M, Kratz K, Lendlein A. Temperature-controlled reversible pore size change of electrospun fibrous shape-memory polymer actuator based meshes. *Smart Mater Struct* **2019**;*28*:055037.
35. Zhao J, Cui W. Functional electrospun fibers for local therapy of cancer. *Adv Fiber Mater* **2020**;*2*:229–45.
36. Wang W, Yu A, Zhai J, Wang ZL. Recent progress of functional fiber and textile triboelectric nanogenerators: towards electricity power generation and intelligent sensing. *Adv Fiber Mater* **2021**;*3*:394–412.
37. Yang X, Li L, Yang D, Nie J, Ma G. Electrospun core-shell fibrous 2D scaffold with biocompatible poly(glycerol sebacate) and poly-l-lactic acid for wound healing. *Adv Fiber Mater* **2020**;*2*:105–17.
38. Herath M, Epaarachchi J, Islam M, Zhang F, Leng J, Fang L, Yan C, Peng GD, Schade W. Remote actuation of light activated shape memory polymers via d-shaped optical fibres. *Smart Mater Struct* **2020**;*29*:047001.
39. Zhang F, Xia Y, Wang L, Liu L, Liu Y, Leng J. Conductive shape memory microfiber membranes with core-shell structures and electroactive performance. *ACS Appl Mater Interfaces* **2018**;*10*:35526–32.
40. Lee J, Kang S-K. Principles for controlling the shape recovery and degradation behavior of biodegradable shape-memory polymers in biomedical applications. *Micromachines* **2021**;*12*:757.
41. Niiyama E, Tanabe K, Uto K, Kikuchi A, Ebara M. Shape-memory nanofiber meshes with programmable cell orientation. *Fibers* **2019**;*7*:20.
42. Wang X, Yan H, Shen Y, Tang H, Yi B, Qin C, Zhang Y. Shape memory and osteogenesis capabilities of the electrospun poly(3-hydroxybutyrate-Co-3-hydroxyvalerate) modified poly(l-lactide) fibrous mats. *Tissue Eng Part A* **2021**;*27*:142–52.
43. Luo X, Mather PT. Shape memory assisted self-healing coating. *ACS Macro Lett* **2013**;*2*:152–6.
44. Pai C-L, Boyce MC, Rutledge GC. Morphology of porous and wrinkled fibers of polystyrene electrospun from dimethylformamide. *Macromolecules* **2009**;*42*:2102–14.
45. Huang T, Zhu Y, Zhu J, Yu H, Zhang Q, Zhu M. Self-reinforcement of light, temperature-resistant silica nanofibrous aerogels with tunable mechanical properties. *Adv Fiber Mater* **2020**;*2*:338–47.
46. Guan X, Chen H, Xia H, Fu Y, Qiu Y, Ni Q-Q. Multifunctional Composite nanofibers with shape memory and piezoelectric properties for energy harvesting. *J Intell Mater Syst Struct* **2020**;*31*:956–66.
47. Zhang F, Liu K, Pan Z, Cao M, Zhou D, Liu H, Huang Y, Duan X. Effects of rosiglitazone/PHBV drug delivery system on postoperative fibrosis in rabbit glaucoma filtration surgery model. *Drug Deliv* **2019**;*26*:812–9.
48. Aydemir Sezer U, Sanko V, Gulmez M, Aru B, Sayman E, Aktekin A, Vardar Aker F, Yanıkkaya Demirel G, Sezer S. Polypropylene composite hernia mesh with anti-adhesion layer composed of polycaprolactone and oxidized regenerated cellulose. *Mater Sci Eng C* **2019**;*99*:1141–52.
49. Guner MB, Dalgic AD, Tezcaner A, Yilanci S, Keskin D. A Dual-phase scaffold produced by rotary jet spinning and electrospinning for tendon tissue engineering. *Biomed Mater Bristol Engl* **2020**;*15*:065014.
50. Ahn S, Chantre CO, Gannon AR, Lind JU, Campbell PH, Grevesse T, O'Connor BB, Parker KK. Soy protein/cellulose nanofiber scaffolds mimicking skin extracellular matrix for enhanced wound healing. *Adv Healthc Mater* **2018**;*7*:e1701175.
51. Johnson R, Ding Y, Nagiah N, Monnet E, Tan W. Coaxially-structured fibres with tailored material properties for vascular graft implant. *Mater Sci Eng C Mater Biol Appl* **2019**;*97*:1–11.

Lu Wang obtained a Bachelor of Engineering from Harbin Engineering University (HEU) in 2020 and now she is a master of the Center for Smart Materials and Structures at Harbin Institute of Technology (HIT), China. Currently, she is focusing on shape memory polymers and their structures, multifunction composites and their applications.

Jingyi Ma obtained a master's degree of Clinical Medicine from Harbin Medical University (HMU) in 2020 and now she is a doctoral student of ophthalmology at The Second Affiliated Hospital of Harbin Medical University, China. Currently, she is focusing on anti-scarring of glaucoma surgery.

Tao Guo obtained a Bachelor of Engineering from Harbin University of Science and Technology (HUST) in 2020 and now he is a master of the Center for Smart Materials and Structures at Harbin Institute of Technology (HIT), China. Currently, he is focusing on shape memory polymers and the design and application of micro- and nano-structures.

Fenghua Zhang is an associate professor in Center for Smart Materials and Structures at Harbin Institute of Technology (HIT), China. She obtained her PhD degree in the field of materials at HIT in 2017. From 2014 to 2016, she as a visiting student does her research work at University of Cambridge supported by CSC. She has published more than 60 SCI scientific papers. Her research interests are focusing on shape memory polymers and their composites, including shape memory polymers with nano/microstructures, 4D printed smart materials and structures for biomedical applications, stimuli methods and multifunctional composite materials.

Aimeng Dong is a medical doctor at Department of Ophthalmology, The 2nd Affiliated Hospital, Harbin Medical University (HMU), China. Prior to her career in medicine, she obtained her PhD degree in the field of glaucoma at HMU in 2019. Her research interests lie in how innovation and technological change to prevent ocular scarring after glaucoma surgery.

Shiqi Zhang is an assistant research fellow in the department of ophthalmology in the Second Hospital of Harbin Medical University, China. And she is also a postdoctoral fellow of college of Pharmacology, Harbin Medical University (HMU). Currently, she is focusing on the research of pathogenesis of glaucoma, and the application research of biomaterials in ophthalmology.

Yanju Liu is a professor in the Department of Aerospace Science and Mechanics at the Harbin Institute of Technology (HIT), China. From 1999 to 2003, she was a research fellow at Nanyang Technological University and Newcastle University. She was invited to serve as an associate editor of the journal of Smart Materials and Structures, a Committee Member of APCSNM and a Committee Member of SAMPE. She is working on smart materials and structures, including electrorheological and magnetorheological fluids, electroactive polymers, and shape memory polymers and their nanocomposites. She has authored or co-authored over 170 scientific papers in different journals.

Huiping Yuan is a professor of ophthalmology and Director of Department of Ophthalmology in the Second Hospital of Harbin Medical University, China. Her research interests cover the clinical and basic research of glaucoma, including the epidemiology, pathogenesis of glaucoma and neuroprotection research. She is a state department special allowance expert, an expert member of Chinese Medical Association. She is also served as the vice Chairman of Ophthalmology Professional Committee of China Medical Women's Association (CMWA), the vice Chairman of Ophthalmology and Visual Science Committee, Chinese Research Hospital Association (CRHA).

Jinsong Leng is a full professor and Director of Center for Smart Materials and Structures at Harbin Institute of Technology, China. His research interests cover shape memory polymers and their composites. He is served as the Vice President of International Committee on Composite Materials (ICCM). He is elected as the Academician of the Chinese Academy of Sciences, Foreign Member of Academia Europaea, Member of the European Academy of Science and Arts, World Fellow of ICCM, Fellow of AAAS, Fellow of SPIE, Fellow of Institute of Physics (IOP), Fellow of Royal Aeronautical Society (RAeS), Fellow of IMMM and Associate Fellow of AIAA.